Loss of neuroglobin expression alters Cdkn1a/Cdk6-expression resulting in increased proliferation of neural stem cells

Loss of neuroglobin-expression alters Cdkn1a/Cdk6-expression resulting in increased proliferation of neural stem cells

Evi Luyckx[1,5] (evi.luyckx@uantwerpen.be), Wendy Van Leuven[1,5] (vanleuven.wendy@gmail.com), Daniel Andre[2] (andred@uni-mainz.de), Alessandra Quarta[3] (alessandra.quarta@uantwerpen.be), Kristien Reekmans[3] (kristien_reekmans@hotmail.com), Erik Fransen[4] (erik.fransen@uantwerpen.be), Luc Moens[1] (luc.moens@uantwerpen.be), Thomas Hankeln[2] (hankeln@uni-mainz.de), Peter Ponsaerts[3] (peter.ponsaerts@uantwerpen.be), Sylvia Dewilde[1] (sylvia.dewilde@uantwerpen.be)

[1] Protein chemistry, Proteomics and Epigenetic Signaling, University of Antwerp, Antwerp, B-2610, Belgium

[2] Institute of Organismic and Molecular Evolution, Molecular Genetics and Genome Analysis, Johannes Gutenberg-University Mainz, Mainz, D-55099, Germany

[3] Laboratory of Experimental Hematology, Vaxinfectio, University of Antwerp, Antwerp, B-2610, Belgium

[4] StatUA Center for Statistics, University of Antwerp, Antwerp, B-2000, Belgium

[5] Co-first author

Running title: Neuroglobin alters cell cycle in neural stem cells

Corresponding author: Sylvia Dewilde (Protein chemistry, Proteomics and Epigenetic Signaling, University of Antwerp, Antwerp, B-2610, Belgium; sylvia.dewilde@uantwerpen.be; +3232652323)

Abbreviations

Ngb	neuroglobin
NSC	neural stem cell
fl	floxed
KO	knockout
Cdkn1a	cyclin-dependent kinase inhibitor p21
Cdk6	cyclin dependent kinase 6
Pten	phosphatase and tensin homolog
ES	embryonic stem cell
NEM	neural expansion medium
EGF	epidermal growth factor
hFGF-2	human fibroblast growth factor-2
BSA	bovine serum albumin
NSPH	neurosphere
GFAP	glial fibrillary acidic protein
TuJ1	beta-3 tubulin
PE	phycoerythrin
DEG	differentially expressed gene
GO	gene ontology
IPA	ingenuity pathway analysis
PCA	principle component analysis

HCA hierarchical cluster analysis

HRP horseradish peroxidase

GD glucose deprivation

OGD oxygen and glucose deprivation

Key words: neuroglobin – cell cycle – transcriptomics – neural stem cells

Abstract

In the quest to unravel its functional significance, neuroglobin (Ngb), a brain-specific neuroprotective protein, has recently been proposed as an actor in neurodevelopment. As neural stem cells (NSCs) are fundamental during brain development, the present study aimed at investigating the role of Ngb in the growth and proliferation of NSCs by comparing an Ngb-floxed (Ngb_{fl}-)NSC line, equivalent to the wild type cellular situation, with an in-house created Ngb knockout (Ngb_{KO}-)NSC line. Ngb_{KO}-NSCs were characterized by an increased growth and proliferation capacity *in vitro*, supported by RNA sequencing and Western blot results reporting the downregulation of Cdkn1a and the upregulation of Cdk6, both enhancing the cell cycle. Based on additional gene ontology enrichment and pathway analyses, we hypothesize that the loss of Ngb affects multiple cellular signaling pathways with the most important being the kt-Tp53 axis.

Introduction

As a member of the globin family, neuroglobin (Ngb) is an oxygen-binding protein that is mainly expressed in neurons of the central and peripheral nervous system. Since its discovery in 2000, many *in vitro* and *in vivo* studies were performed to scrutinize the functional significance of this highly conserved protein [1-3]. To date, Ngb is considered to act neuroprotectively since it is induced upon neuronal hypoxia and cerebral ischemia and protects neurons in oxygen-deprived conditions caused for example by traumatic brain injury or neurodegenerative disorders [4-8]. Although the molecular mechanism behind Ngb's neuroprotective character still remains to be elucidated, various hypotheses have been proposed. These molecular actions include enhancing O_2 supply to the mitochondria of metabolically active neurons, preventing apoptosis and scavenging reactive oxygen and nitrogen species and thereby reducing oxidative stress [2]. More recently, Ngb gained growing interest in the field of neurodevelopment. While early stages of mouse brain development are characterized by low-level Ngb mRNA and protein expression, Ngb levels steadily rise from the late prenatal days to brain maturing newborns and even further to young adults, presenting the protein as a potential key player during brain development [9, 10]. Additionally, Ngb co-expression with Sox-3 and Sox-4, involved in the preservation of progenitor neuronal cells, in the neurogenic subventricular zone in adult rat brain supports a potential role of Ngb in neural stem cell (NSC) migration, proliferation and neurogenesis [11-13]. Recent molecular evidence even states an interaction of Ngb with phosphatase and tensin homolog (Pten) and Akt which leads to prominent effects in the Pten/PI3K/Akt signaling cascade suggesting a role of Ngb in neuritogenesis and neuronal development in general [14].

NSCs are of great value to investigate the role of Ngb in different stages of neurodevelopment. In the present study, we first generated an Ngb-floxed (Ngb_{fl}) mouse model by introducing *loxP* sites into the introns flanking exon 2 and 3 of the *Ngb* locus. From this mouse model, we cultured embryonic brain-derived NSCs (Ngb_{fl}-NSCs), followed by *in vitro* Cre-lox recombination to obtain an Ngb knockout (Ngb_{KO}-)NSC line. A comparative *in vitro* study combined with transcriptome analysis of both Ngb_{fl}-NSC and Ngb_{KO}-NSC lines was performed and validated on the protein level, thereby identifying Ngb-associated up- and downregulation of cell cycle proteins.

Materials and Methods

Mice

The Ngb knockout model was created using Cre-lox recombination. The development of the *Ngb-floxed* mouse model, containing two *loxP* recombination sites flanking critical regions of the *Ngb* gene, was performed by GenOway under the project no. genOway/EV/MOE-1-NGB/120307. In brief, using 129Sv/Pas embryonic stem (ES) cell DNA, a targeting vector consisting of 8.9 kb of mouse genomic DNA (gDNA) containing the entire *Ngb* gene locus supplemented with a *loxP* site in intron 1 and a validated *FRT-neomycin-FRT-loxP* cassette in intron 3 was constructed in our lab. Next, after transfection via standard electroporation procedures, the linearized targeting construct was introduced into the mouse genome by homologous recombination in 129Sv/Pas ES cells (GenOway). Recombinant clones resistant to G418 were validated by genomic PCR and Southern blot. To obtain chimeric mice, positive selected recombinant ES cells were injected into C57BL/6 recipient blastocysts, isolated from pregnant C57BL/6 females. Thereafter, chimeric mice were mated with C57BL/6 mice and subsequently with C57BL/6 Flp mice (GenOway) to allow germ line excision of the neomycin selection cassette. Speed congenic backcrossing to C57BL/6 was performed. The Max-Bax single nucleotide polymorphism (SNP) panel (Charles River) was used to screen animals with the highest percentage of recipient versus donor strain DNA. After 5 crossings, the background was 99.73 % C57BL/6. These mice are defined as *Ngb-floxed* mice (Ngb^{fl}).

All mice were bred in the animal facility of the University of Antwerp. Animals were housed in a temperature controlled room with day-night cycle (12/12) and free access to food and water. All experiments were conducted in compliance with the guidelines from Directive 2010/63/EU of the European Parliament on the protection of animals used for scientific purposes and all experiments were approved by the Ethics Committee of the University of Antwerp.

Neural stem cell cultures

NSCs were cultured from the embryonic brain of a male Ngb^{fl} embryo of 14 to 16 days *postcoitus* following a protocol previously described [15] with minor modifications [16]. Briefly, the embryonic brain was enzymatically dissociated using a 0.2 % collagenase A (Roche)/DNase-I (1000 Kunitz/50 ml, Sigma) solution in phosphate-buffered saline (PBS) for 2 h at 37 °C in a shaking water bath. The cell population obtained was then resuspended in 10 ml neural expansion medium (NEM), consisting of Neurobasal A medium (Invitrogen) supplemented with 10 ng/ml epidermal growth factor (EGF, ImmunoTools), 10 ng/ml human fibroblast growth factor-2 (hFGF-2, ImmunoTools), 100 U/ml penicillin

(Invitrogen), 100 mg/ml streptomycin (Invitrogen), 0.5 µg/ml amphotericin B (Invitrogen), and 1 % modified N2 supplement. The modified N2 supplement consisted of DMEM/F12 medium (Gibco) supplemented with 7.5 mg/ml bovine serum albumin (BSA, Invitrogen), 2.5 mg/ml insulin (Sigma), 2 mg/ml apo-transferrin (Sigma), 0.518 µg/ml sodium selenite (Sigma), 1.6 mg/ml putrescine (Sigma) and 2 µg/ml progesterone (Sigma). Cells were plated in a T25 culture flask in order to obtain a neurosphere (NSPH) population. Next, NSPHs were dissociated using accutase (Sigma) and cells were plated in 10 ml NEM on fibronectin-coated (5 µg/ml in PBS, R&D Systems) T25 culture flasks to allow outgrowth of an adherently growing NSC culture. Following 24 h of culture, non-adherent cells were removed and 10 ml fresh NEM was added to the cultures. After 7 days, cultured cells were harvested following accutase (Sigma) treatment for 5 minutes at 37 °C and seeded in a new fibronectin-coated T25 flask in 10 ml NEM (passage 1). For routine cell culture, NEM was replaced each 3-4 days and NSC cultures were split 1:5 every 7 days. Cell cultures were incubated at 37 °C and 5 % CO_2. NSCs derived from Ngb_{fl} mice are defined as Ngb_{fl}-NSCs.

mRNA lipofection of neural stem cell cultures

mRNA encoding the Cre recombinase protein was prepared as described previously [17, 18] and mRNA lipofection was performed following the protocol of Reekmans et al. [16]. Directly prior to mRNA lipofection, fresh mRNA (5µg)/Lipofectamine™ 2000 (10 µl) mixtures were prepared in 600 µl OptiMem medium (Invitrogen), according to the manufacturer's instructions. Next, subconfluent (70 %) T25 flask cultures of NSCs were washed twice with PBS and fresh NEM without antibiotics (10 ml) and mRNA lipoplexes (600 µl) were added to the cultures. After 4 h, medium was refreshed to remove remaining lipoplexes. Confluent cultures were harvested, partially used to extract gDNA to verify *Cre*-mediated excision, and seeded in T25 flasks. Ngb_{fl}-NSCs which underwent excision of the *Ngb-floxed* locus were considered as Ngb knockout (KO) cells and defined as Ngb_{KO}-NSCs.

gDNA extraction and genotyping

gDNA extraction was performed using the Wizard SV Genomic DNA Purification System (Promega) according to the manufacturer's instructions. To identify the presence of two *Ngb-floxed* alleles, a polymerase chain reaction (PCR) was performed using 50 ng forward primer Fin1loxP (5'-TCATTCCCCCAGATTCTGAT-3'), annealing upstream of the distal *loxP* site, and 50 ng reverse primer Rin1loxP (5'-AAACGGGCAATAGCATCAAG-3'), annealing downstream of the distal *loxP* site. In the presence of *loxP* sites, an amplified product of 279 bp is expected. Intermediate and final targeting vectors were used as negative controls. PCR was performed using Taq DNA

polymerase (Life Technologies) according to the manufacturer's instructions following a 2 minutes incubation on 94 °C before proceeding to 35 cycles of 94 °C for 30 seconds, 55 °C for 30 seconds and 72 °C for 1 minute, ending with an incubation of 10 minutes on 72 °C. Lengths of amplicons were compared to a GeneRuler 1 kb DNA ladder (ThermoFisher Scientific) on a 1.5 % agarose gel.

To evaluate the excision of the *Ngb-floxed* locus, a PCR was performed targeting the full *Ngb-floxed* locus by Fin1loxP (5'-TCATTCCCCCAGATTCTGAT-3') and reverse primers annealing exon 4, Rex4 (5'-ACCACAGCTCCGTAGAGTCG). Successful Cre-lox recombination results in the excision of the *Ngb-floxed* locus and an amplified product of approximately 960 bp. PCR was performed using the expand long template kit (Roche) according to the manufacturer's instructions following a 2 minutes incubation on 94 °C before proceeding to 35 cycles of 94 °C for 30 seconds, 56 °C for 1 minute and 68 °C for 5 minutes, ending with an incubation of 10 minutes on 68 °C. To assess the gender of the NSC line used in this study, isolated gDNA was used in a mouse sex genotype PCR which was carried out as described in literature [19]. Lengths of amplicons were compared to a GeneRuler 1 kb DNA ladder (ThermoFisher Scientific) on a 1 % agarose gel.

mRNA extraction

Cell pellets of Ngb_{KO}-NSCs and Ngb_{fl}-NSCs of three consecutive passages were treated with TriReagent (Sigma) for 10 minutes at room temperature. Additionally chloroform (Merck) was added and after 10 minutes samples were centrifuged at 13 400 g for 15 minutes at 4 °C. The upper RNA containing transparent layer was collected and processed with the PureLink RNA mini kit (Ambion) according to the manufacturer's instructions, including an on-column DNase I digestion using the PureLink DNase Set (Life Technologies). RNA concentration and integrity were analyzed using the Qubit RNA HS Assay (Life Technologies) and BioAnalyzer total RNA Nano Chip (Agilent) respectively.

Real-time quantitative PCR

First strand cDNA synthesis was performed on 1 µg total RNA with the SuperScript III reverse transcriptase (Invitrogen) according to the manufacturer's instructions. For validation of *Ngb* expression levels, qRT-PCR was carried out on the ABI Prism 7500 Fast and 7000 Sequence Detection Systems (Applied Biosystems). Each real-time PCR reaction comprised the amount of cDNA equivalent to 25 ng of total RNA in a 10 µl reaction containing SYBR Green (GoTaq Real-Time Master Mix, Promega) with 0.33 µM of each primer targeting *Ngb* (Ngb-qPCR-For: 5´-

GCTCAGCTCCTTCTCGACAG-3´;Ngb-qPCR-Rev: 5´-CAACAGGCAGATCAACAGAC-3´) or *Rplp0* (Rplp0-qPCR-For : 5‘-AGGGCGACCTGGAAGTCC-3‘; Rplp0-qPCR-Rev: 5‘- GCATCTGCTTGGAGCCCA-3‘). The parameters for amplification were 95 °C for 15 seconds, 58 °C for 30 seconds, 72 °C for 30 seconds, measuring the fluorescence during the last step of each cycle. The standard-curve approach by measuring Ct-values was used to calculate mRNA levels. Assay performance was calculated by a serial dilution of a standard-plasmid containing the amplicon sequence. Quantification of *Ngb* was carried out using the absolute quantification method with serial dilutions of a known standard to calculate copy numbers per µg RNA.

Astrocyte and neuronal differentiation of neural stem cells

For differentiation of NSCs to astrocytes, NSCs were plated in 1 ml Neurobasal A medium (Invitrogen) supplemented with 1 % modified N2 supplement and 1 % fetal calf serum (Gibco) in a density of 15 000 cells/cm^3 on fibronectin-coated (5 µg/ml in PBS, R&D Systems) cover slips. For neuronal differentiation, NSCs were plated in 1 ml Neurobasal A medium (Invitrogen) supplemented with 1 % fetal calf serum (Gibco), 2 % B-27 (Gibco) and 2 ng/ml human fibroblast growth factor-2 (hFGF-2, ImmunoTools) in a density of 10 000 cells/cm^3 on poly-L-ornitin (15 µg/ml in PBS, Sigma)/laminin (10 µg/ml in PBS, Sigma)-coated cover slips. Cells were cultured for 11 days and half of the medium was replaced every 2-3 days.

Glucose deprivation induced cell death under normoxia and anoxia

Following seeding of cells in triplicate in a 6-well plate with a density of 1 x 10^5 cells per well, medium was refreshed after 24 hours and cells were incubated with glucose deprived medium, under normoxic or anoxic (5 % CO, 95 % N_2) conditions for 24 or 48 hours. Anoxia was achieved using a humidified Bactron IV anaerobic chamber (Shel Lab) as described [20]. Confirmation of the stability of O_2 tension in the gas phase at < 0.1 % O_2 was obtained by a Greisinger GMH3691 air oximeter (Metresys). After normoxia or anoxia, cells were harvested, counted manually in a Neubauer chamber and cell viability was measured by flow cytometry. Normalization was carried out using values of the starting point (100 %).

Flow cytometry

Cell viability of at least 1 x 10^4 cells per sample was evaluated on an Epics XL-MCL analytical flow cytometer (Beckman Coulter) using GelRed® (1x final concentration, Biotum). Flow cytometric data were analyzed using FlowJo software (LLC).

Growth curve analysis

Cells were plated in a 6-well culture dish in triplicate in a density of 5 x 10^4 cells/well. After accutase (Sigma) treatment, cells were counted manually in a Neubauer chamber. The number of cells was recorded daily over a 4-day period. Normalization was carried out using values of the starting point (100 %).

Immunofluorescence microscopy

Immunofluorescent staining of undifferentiated and differentiated NSCs was performed using following antibodies: a polyclonal rabbit anti-glial fibrillary acidic protein antibody (anti-GFAP, 1/1000, Abcam ab7779) in combination with an FITC-labelled goat anti-rabbit secondary antibody (1/200, Jackson ImmunoResearch 111-096-045) and a monoclonal mouse anti-mouse neuron-specific beta-3 tubulin antibody (anti-TuJ1, 1/200, R&D Systems MAB1195) in combination with an AlexaFluor 555-labelled goat anti-mouse secondary antibody (1/200, Invitrogen A21425) for differentiation experiments and with a phycoerythrin (PE)-labelled anti-Ki67 antibody (1/20, BD 556027) for anti-Ki67 staining. Cell cultures grown on cover slips were washed with TBS, fixated with 4 % paraformaldehyde in TBS for 20 minutes at room temperature (RT), washed again with TBS and incubated with 0.1 % Triton-X-100 (Sigma) in TBS for 30 minutes. Next, cover slips were incubated for 1 hour at RT with goat serum (1/5, Jackson ImmunoResearch) in TBS for anti-GFAP staining or with goat serum (1/5, Jackson ImmunoResearch) and AffiniPure Fab Fragment Goat anti-Mouse IgG (H+L) (1/100, Jackson ImmunoResearch) in TBS for anti-TuJ1 and anti-GFAP double staining or for 1 hour at 37 °C with 3 % BSA and AffiniPure Fab Fragment Goat anti-Mouse IgG (H+L) (1/250, Jackson ImmunoResearch) for anti-Ki67 staining. After washing with TBS, cover slips were incubated overnight at 4 °C with primary antibody in 10 % milk powder. For anti-GFAP and anti-TuJ1 staining, cover slips were washed with TBS and incubated for 1 hour on RT with secondary antibodies. After washing with TBS, cover slips were incubated for 10 minutes at RT with 4', 6-diamidino-2-phenylindole (DAPI, 1/1000, Sigma) in TBS. After a final washing step with demineralized water, cover slips were mounted with ProLong® Gold antifade reagent (Life Technologies). Visualization of immunostained cells was performed using a standard fluorescence microscope (Olympus BX51)

equipped with an Olympus DP71 digital camera. Olympus Cell-F Software was used for image acquisition and processing. Images for Ki67 staining were analyzed with TissueQuest software (TissueGnostics).

Assay for cell cycle distribution

Cells were plated in a density of 5500 cells/cm^2 in NEM and cultured for 5 days until 80 – 90 % confluency was reached. Cell cycle distribution was evaluated using Cycletest^{TM} Plus DNA kit (BD Biosciences) on an Epics XL-MCL analytic flow cytometer (Beckman Coulter) and analyzed with FlowJo (LLC).

RNA-Sequencing library preparation and Illumina sequencing

Total extracted RNA from Ngb$_{KO}$-NSCs and Ngb$_{fl}$-NSCs was used for RNA-Seq library preparation. Libraries were generated by StarSEQ (Mainz, Germany) using the Illumina TrueSeq RNA sample preparation Kit v.2 (Illumina). Each library was prepared using 825 ng of total RNA. Sequencing was performed on an Illumina HiSeq 2500 instrument in rapid mode employing a paired-end, 100 bp read length sequencing strategy. RNA-Seq data are available at the European Nucleotide Archive under accession number PRJEB20351.

Data processing and RNA-Seq mapping procedure

The FASTX–Toolkit (http://hannonlab.cshl.edu/fastx_toolkit/index.html) was used for quality filtering and adapter trimming. The first 15 bp of each read were clipped. Reads shorter than 20 nucleotides and reads that possessed phred score's smaller than 20 for more than 20 percent of the read were discarded. Quality assessment of the Illumina RNA-Seq reads was performed using the FastQC software (http://www.bioinformatics.fbabraham.ac.uk/projects/fastqc/) prior and after the trimming procedure. FASTQ files were imported into the CLC Genomics Workbench version 7.5 (CLC Bio-Qiagen, Aarhus, Denmark) and mapped against the gene regions of the mouse reference genome build 38 (GRCm38). For read-mapping the alignment cost parameters were set as follows: mismatch cost 2, insertion cost 3 and deletion cost 3. For filtering the resulting alignments, only mapped reads were included in the output, if at least 95 % of the read length matched the reference sequence with an identity of at least 95 %. Furthermore, only reads were retained which mapped uniquely against one specific region in the reference genome.

Differential gene expression analysis

To identify differentially expressed genes (DEGs) in the dataset, the number of total exon reads for each gene and for both conditions were extracted from the RNA-Seq mapping together with the corresponding official gene symbols. Based on these read-count data we performed a differential gene expression analysis using the DESeq Bioconductor package version 1.18.0 [21] within R version R-3.1.2 (www.r-project.org) for statistical computing. In absence of biological replicates for each condition, the 'blind' method for computing the empirical dispersion with the settings: fitType: 'local' and SharingModel 'fit-only' were used as described in the DESeq vignette for working without replicates (http://www.bioconductor.org/packages/devel/bioc/vignettes/DESeq/inst/doc/DESeq.pdf). DEGs were identified using a Benjamini-Hochberg (BH) adjusted P-value at a significance level of $P < 0.05$.

Functional enrichment and pathway analysis

Gene Ontology (GO) enrichment analysis was performed separately for up- and downregulated genes using the WEB-based Gene SeT AnaLysis Toolkit (WebGestalt) [22, 23]. The whole mouse genome was set as reference. To determine statistically enriched terms, the hypergeometric method combined with a more conservative Bonferroni P-value correction ($P < 0.01$) was used for statistical testing. Furthermore only statistically enriched terms that comprised at least 4 genes of the input dataset were selected. To conduct Ingenuity Pathways Analysis (IPA) (Qiagen; www.ingenuity.com), we imported all identified DEGs into IPA together with their corresponding fold changes and BH-corrected P-values and performed a core analysis with default settings. Significant canonical pathways were determined by using Fisher's exact test with a P-value threshold of $P < 0.01$.

RT^2 profiler PCR array

As a validation of the results extracted from RNA-Seq and to identify potential differently expressed cell cycle genes, RT^2 profiler cell cycle PCR arrays (Qiagen) were applied according to manufacturer's instructions. Potential up- and downregulated genes were selected via the online provided tools (Qiagen).

Principle component (PCA) and hierarchical clustering analyses (HCA)

To confirm that the cells used in this study can be clearly termed as NSCs, PCA and HCA were performed using our own and additional public available transcriptome datasets from different cells types of the mouse brain (astrocytes, neurons, NSCs, NSPHs, oligodendrocytes and oligodendrocyte progenitor cells). The following RNA-Seq datasets

were included in the analysis and downloaded as FASTQ-Files from the Sequence Read Archive of NCBI: SRX861703, SRX2588589, SRX380380, SRX380382, SRX380384, SRX380386, SRX539543, SRX591754 and SRX1620324. Trimming, quality filtering and mapping of the reads were done within the CLC Genomics Workbench version 9.0 (CLC Bio Qiagen, Aarhus, Denmark) using the same parameters as already described. All subsequent analysis and calculations were done in R (v.3.4.2). PCA and HCA were carried out on the log-transformed normalized counts using the rlogTransformation function of the DESeq2 package (v.1.18.1). PCA was further calculated by using the plotPCA function of DESeq2 with default settings and visualized via the ggplot2 package (v.2.2.1). Hierarchical clustering analyses were performed based on a Pearson correlation distance of a subset of known marker genes for NSCs, astrocytes, and cells of the neuronal and oligodendroglial lineage by using the *cor* and *hclust* commands in R and drawn via the heatmap.2 function of the gplots package (v.3.0.1). The following marker genes were included in the analysis: NSC-markers *Abcg2*, *Ascl1*, *Fabp7*, *Hes1*, *Nes*, *Pax6*, *Slc1a3*, *Sox2*, *Sox3*, *Sox9* and *Vim*; astrocyte-specific markers *Acsbg1*, *Aldh1l1*, *GFAP* and *Gli3*; neuronal linage markers *Dcx*, *Dlx2*, *Eomes*, *Gad1*, *Map2*, *Rbfox3*, *Syt1*, *Syp*, *Tbr1*, *Tubb3*; oligodendroglial lineage markers *Mbp*, *Mobp*, *Mag* , *Mog*, *Olig2*, *Plp1* and *Sox10* [24-31].

Western blot

NSCs were harvested by accutase treatment (Sigma) and incubated on ice for 5 minutes with N-PER™ Reagent (ThermoFisher Scientific) supplemented with cOmplete™ Mini Protease Inhibitor Cocktail (Roche) following the manufacturer's instructions and centrifuged at 10 000 g for 10 minutes to obtain whole-protein extracts. Total protein concentration was determined using the Pierce™ BCA Protein Assay kit (ThermoFisher Scientific). The protein extracts (50 µg for Cdkn1a, Akt, P-Akt$_{SER}$, P-Akt$_{THR}$ and 130 µg for Cdk6) and the PageRuler™ Plus Prestained Protein Ladder (ThermoFisher Scientific) were subjected to 12,5 % SDS-PAGE and transferred to a Immobilon®-P PVDF membrane (Millipore). The membrane was blocked for 1 hour on RT with 5 % milk powder in TBS and incubated overnight on 4 °C with primary antibody (monoclonal mouse anti-β-Actin (1/10 000, Sigma A1978), monoclonal rabbit anti-Cdkn1a (1/1000, Abcam ab109199) or monoclonal mouse anti-Cdk6 (1/2000, Cell Signaling #3136)) in 5 % milk powder and 0.1 % Tween-20 (Sigma) in TBS or with primary antibody (monoclonal rabbit anti-Akt (1/1000, Cell Signaling #4691), monoclonal rabbit anti-P-Akt$_{SER}$ (1/2000, Cell Signaling #4060), polyclonal rabbit anti-P-Akt$_{THR}$ (1/1000, Cell Signaling #9275)) in 5 % BSA (Sigma) and 0.1 % Tween-20 (Sigma) in TBS. After washing with TBS, the membrane was incubated for 1 hour on RT with secondary antibody (Horseradish Peroxidase (HRP)-conjugated polyclonal goat anti-mouse antibody (1/1000, Dako P0447) or HRP-conjugated polyclonal goat anti-rabbit antibody

(1/2000, Dako P0448)) in TBS. After washing with TBS, Luminata Forte Western HRP Substrate (Millipore) was added to the membrane and targeted proteins were visualized using a G:BOX (SynGene) imager and analyzed using GeneSnap and ImageJ.

Statistical analysis

Levels of *Ngb* copy number (Fig. 1C) were analyzed using independent samples t-test using GraphPad Prim 6.0. The effect of oxygen treatment and genotype on the percentage of growth was modelled using multiple linear regression (Fig. 3). The percentage surviving cells, after normalization, was entered as dependent variable. Genotype, time and oxygen were entered as independent variables. Since the change over time followed an approximately linear pattern, time was entered as a continuous variable. The multiple regression model was fitted by stepwise backward elimination, starting from a full model with all interaction terms, and eliminating non-significant terms in each step. The difference in the growth pattern (Fig. 4A) was analyzed using a two-way ANOVA model, the difference in mean growth between the 2 genotypes at each separate day was analyzed using independent samples t-tests. For the Ki67 immunostaining (Fig. 4B), the relation between the Ki67 labelling index and the genotype of NSCs was modelled with a linear mixed model, adding a random intercept term to account for the non-independence between observations within the same cover slip. Linear mixed models were fitted using the lme4 package in the statistical package R, version 3.1.0 (www.r-project.org). Significance of the genotype effect was tested using the F-test with the Kenward-Roger correction, as implemented in the pbkrtest package. The *posthoc* test was carried out using the package multcomp, with the Tukey correction for multiple testing. Cell cycle distribution (Fig. 4C) was analyzed by Mann-Whitney U tests in GraphPad Prism 6.0. Western blot assays (Fig. 5 B-C) were normalized to β-Actin expression where after the signal in Ngb_{KO}-NSC extracts was normalized to the signal of Ngb_{fl}-NSC extracts. Therefore, Wilcoxon signed-rank tests were used to analyze the normalized data. In general $P < 0.05$ indicated statistical significance.

For transcriptomics, statistics on RNA-Seq data processing, DEGs, IPA, PCA and HCA were described in the respective sections. Expression levels obtained by the RT^2 profiler array were analyzed by independent samples t-tests. In general $P < 0.05$ indicated statistical significance.

Results

Generation of an Ngb$_{fl}$- and an Ngb$_{KO}$-NSC line from a new mouse model

A new mouse model was created, in which *Ngb* was targeted by introducing *loxP* sites into the introns flanking exon 2 and 3 of the *Ngb* locus (the Ngb$_{fl}$ locus, see Fig. 1A). Since exons 2 and 3 encode the heme pocket together with two histidine codons known to be essential for the correct folding and activity of the Ngb protein, targeting this region leads to a loss of function of Ngb after Cre-lox recombination [1, 32]. Ngb$_{fl}$-NSCs were isolated from the brain of an Ngb$_{fl}$ embryo and lipofected with *Cre* recombinase-encoding mRNA to obtain the Ngb$_{KO}$-NSC line. PCR analysis on gDNA extracts from Ngb$_{fl}$- and Ngb$_{KO}$-NSCs clearly showed the absence of the Ngb$_{fl}$ allele in the latter, confirming the desired excision of exon 2 and 3 by Cre-lox recombination (Fig. 1B). As qRT-PCR analysis showed an *Ngb* copy number of 2.67E+05 ± 0.37E+05 per µg RNA of Ngb$_{fl}$-NSCs while *Ngb* expression was absent in Ngb$_{KO}$-NSCs ($P < 0.0001$), the latter was considered as a valid Ngb knockout cell line (Fig. 1C).

Characterization of Ngb$_{fl}$- and an Ngb$_{KO}$-NSC lines

In order to demonstrate that cultured Ngb$_{fl}$- and Ngb$_{KO}$-NSCs have the capacity to differentiate into both glial (GFAP$^+$ astrocytes) and neuronal (TuJ1$^+$ neurons) cell lineages, *in vitro* differentiation was performed (Fig. 1D). While undifferentiated Ngb$_{fl}$- and Ngb$_{KO}$-NSCs were not immuno-reactive for GFAP or TuJ1, *in vitro* differentiated Ngb$_{fl}$- and Ngb$_{KO}$-NSCs clearly showed the morphological presence of astrocytes and neurons. Astrocyte-differentiated Ngb$_{fl}$- and Ngb$_{KO}$-NSCs were both immuno-reactive for GFAP, but not for TuJ1, while neuronally-differentiated Ngb$_{fl}$- and Ngb$_{KO}$-NSCs were immuno-reactive for TuJ1 but not for GFAP. In addition, to confirm the cellular identity of our NSC preparations, we characterized the transcriptional profile of undifferentiated Ngb$_{fl}$- and Ngb$_{KO}$-NSCs in comparison to expression profiles of NSC populations, astrocytes, oligodendrocytes and their progenitor cells, as well as mature neurons using public RNA-Seq datasets. All RNA-Seq data were mapped to the mouse reference genome and reads were counted and normalized. RNA-Seq profiles of the sampled datasets were then compared using two different approaches: a principle component analysis (PCA) and an unsupervised hierarchical cluster analysis (HCA). The PCA (Fig. 2A) showed that the two NSC lines grouped with NSCs and NSPHs obtained in three other, independent studies. This can be interpreted as strong indication of a true NSC identity of Ngb$_{fl}$- and Ngb$_{KO}$-NSCs. Secondly, an unsupervised HCA was performed based on a subset of published marker genes for NSCs, astrocytes, neurons and oligodendrocytes (Fig. 2B). Based on the expression of established marker genes, Ngb$_{fl}$- and Ngb$_{KO}$-NSCs again

showed a consistent grouping with the NSCs and NSPHs from other published studies. Furthermore, the HCA showed that established markers for radial glia-like neural stem cells (e.g. *Sox2*, *Fabp7*, *Slc1a3*, *Olig2* and *Vim* [15]) were clearly enriched as strongly expressed genes in Ngb_{fl}- and Ngb_{KO}-NSCs. Furthermore, the analysis also implied that the Ngb_{fl}- and Ngb_{KO}-NSCs did not undergo further differentiation since genes such as *Eomes/Tbr2*, *Dcx* and *Dlx2*, which are known to be markers for intermediate progenitors or neuronal differentiation [26, 33-36] were only very weakly expressed. Overall, these data demonstrate that loss of Ngb expression does not influence (stem) cell identity and differentiation capacity of NSCs.

NSC mortality following glucose deprivation under normoxia and anoxia was not affected by the absence of Ngb

Ngb_{fl}- and Ngb_{KO}-NSCs were subjected to glucose deprivation under normoxia (GD) and under hypoxia (OGD) for 24 and 48 hours. The effect of oxygen treatment and genotype on the percentage of growth was modelled using multiple linear regression. The final model included significant interaction terms between genotype and oxygen ($P < 0.001$), and between time and oxygen ($P < 2E\text{-}16$), but no significant interaction between genotype and time ($P = 0.42$). This means that OGD, but not GD, significantly reduced cell survival over time resulting in almost total mortality after 48 hours without noticeable differences between Ngb_{fl}- and Ngb_{KO}-NSCs lines (Fig. 3).

Ngb_{KO}-NSCs display enhanced cell proliferation as compared to Ngb_{fl}-NSCs

As glucose-deprived Ngb_{KO}-NSCs displayed some degree of increased proliferation, although not significant, under normoxia compared to Ngb_{fl}-NSCs after 24 hours (115 ± 20 % Ngb_{fl}-NSCs versus 139 ± 23 % Ngb_{KO}-NSCs; Fig. 3, GD condition) and after 48 hours (149 ± 26 % Ngb_{fl}-NSCs versus 186 ± 13 % Ngb_{KO}-NSCs; Fig. 3, GD condition), a deregulation of the growth pattern in Ngb_{KO}-NSCs was suggested. A growth curve analysis of both NSC lines indeed revealed a significantly different growth pattern in Ngb_{KO}-NSCs compared to Ngb_{fl}-NSCs ($P < 0.001$) characterized by consistently significant higher cell numbers at each of the 4 days in Ngb_{KO}-NSCs ($P < 0.01$) (Fig. 4A). Analysis of the proliferation capacity by anti-Ki67 staining confirmed the significantly higher proliferation potential of Ngb_{KO}-NSCs compared to Ngb_{fl}-NSCs ($P < 0.001$) with 57.6 ± 5.4 % Ki67-labelled Ngb_{KO}-NSCs and only 24.6 ± 6.7 % Ki67-labelled Ngb_{fl}-NSCs (Fig. 4B). Additionally, we assessed cell cycle distribution over G0/G1, S and G2/M phases in Ngb_{fl}- and Ngb_{KO}-NSC lines to evaluate changes in the length of a specific cell cycle phase. However, loss of Ngb did not alter cell cycle phase distribution ($P = 0.4$ for G0/G1 phase, $P = 0.2$ for S phase, $P = 0.7$ for G2/M phase) (Fig. 4C).

Ngb$_{KO}$-NSCs showed altered expression of cell cycle genes

Illumina RNA sequencing based on total extracted RNA from Ngb$_{fl}$-NSCs and Ngb$_{KO}$-NSCs obtained 42 - 45 million raw sequence reads for each cDNA library. RNA-Seq data are available at the European Nucleotide Archive under accession number PRJEB20351. Using the CLC Genomic Workbench (version 7.5) for mapping against the mouse reference genome (build GRCm38), 71.8 – 77.5 % of the trimmed and quality filtered reads uniquely mapped to the genome. Using DESeq to identify differential expressed genes with an adjusted P-value threshold of $P < 0.05$, the Ngb$_{KO}$-NSCs demonstrated 55 upregulated genes and 116 downregulated genes with fold-changes of at least 5.6 compared to the Ngb$_{fl}$-NSCs. The most significantly upregulated genes included insulin-like growth factor 2 mRNA binding protein 3 (*Igf2bp3*), zinc finger DBF-type containing 2 (*Zdbf2*), cartilage oligomeric matrix protein (*Comp*), fibronectin type III domain containing 3C1 (*Fndc3c1*) and dorsal inhibitory axon guidance protein (*Draxin*) (Table 1). The most significantly downregulated genes, ranked by adjusted P-value, were: annexin A3 (*Anxa3*), DNA-damage-inducible transcript 4-like (*Ddit4l*), six3 opposite strand transcript 1 (*Six3os1*), transferrin (*Trf*) and interferon-induced protein with tetratricopeptide repeats 3 (*Ifit3*) (Table 1). In agreement with the observed augmented growth and proliferation in Ngb$_{KO}$-NSCs compared to Ngb$_{fl}$-NSCs, a clear up-regulation of the cyclin dependent kinase 6 (*Cdk6*) and an intense downregulation of the cyclin-dependent kinase inhibitor p21 (*Cdkn1a*), both important cell cycling genes, could be revealed ($P < 0.01$) in Ngb$_{KO}$-NSCs (Table 1).

Quantification and validation of up- and downregulated cell cycle genes by an RT^2 profiler PCR array confirmed enhanced cell growth by showing significant upregulation of *Cdk6* in Ngb$_{KO}$-NSCs compared to Ngb$_{fl}$-NSCs ($P < 0.05$). Additionally, *Cdc7* and *Ccna1* were upregulated, though not significantly. Also confirming the RNA-Seq data, *Cdkn1a* proved significantly downregulated in Ngb$_{KO}$-NSCs compared to Ngb$_{fl}$-NSCs ($P < 0.05$) (Fig. 5A). In order to confirm the altered expression of *Cdk6* and *Cdkn1a* on protein level, Western blot experiments were carried out (Fig. 5B-C). Total protein extracts of Ngb$_{KO}$-NSCs showed a clear and significant decrease of Cdkn1a expression ($P < 0.05$) and a moderate, but significant increase of Cdk6 expression compared to the Ngb$_{KO}$-NSCs extracts ($P < 0.05$) (Fig. 5B-C), thus supporting the RNA-Seq and RT^2 profiler transcript analyses.

Developmental processes were upregulated in Ngb$_{KO}$-NSCs

Using the WebGestalt tool, a gene ontology (GO) enrichment analysis based on functional annotations for each differentially expressed gene (DEG) yielded 29 significantly overrepresented biological processes for up-regulated

DEGS and 21 for down-regulated DEGs ($P < 0.01$) (Table S1A - B). For upregulated DEGs, the predominant overrepresented terms were related to developmental processes like 'anatomical structure development' ($P < 0.01$), 'neurogenesis' ($P < 0.01$), and 'cell-, tissue-, organ- or nervous system development' ($P < 0.01$). In contrast, the GO enrichment indicated that downregulated genes in the Ngb_{KO}-NSCs were mainly associated with biological terms that are predominantly involved in inflammatory- or immune response-related processes. Terms like 'innate immune response' ($P < 0.01$), 'response to stress' ($P < 0.001$), 'response to interferon alpha' ($P < 0.01$) or 'beta' ($P < 0.01$) were significantly enriched.

Ingenuity pathway analysis suggested an interplay between Ngb and signaling pathways

To investigate if the observed DEGs are associated with common canonical pathways based on known interactions among them, an Ingenuity Pathway Analysis (IPA) was carried out. IPA revealed 13 statistically significant canonical pathways ($P < 0.01$), most of them involved in cellular signaling processes (Table 2). Among those, the Tp53 signaling pathway was the most significant one, characterized by a common feature of multiple ingenuity canonical pathways: a decrease of *Cdkn1a* expression in Ngb_{KO}-NSCs compared to Ngb_{fl}-NSCs, which could be confirmed on the protein level (Fig. 5B-C), and an increase in *Akt3* expression in Ngb_{KO}-NSCs. To explore the altered expression of Akt or phosphorylated (P)-Akt on the protein level, Western blot experiments were carried out. No significant alterations in the overall Akt, P-Akt_{SER} or P-Akt_{THR} levels could be demonstrated so far (Fig. S1).

Discussion

The development of NSC lines from Ngb_{KO} and Ngb-proficient mice is of great value for unravelling a potential effect of Ngb expression on NSC growth characteristics and pathways. As low or high expression levels of Ngb may point to distinct functions of Ngb in specific brain regions [9], it is important to note that this study primarily addresses Ngb function in low-level expressing cells, taking into account the relatively weak expression of the *Ngb* transcript in NSCs (2.67E+05 ± 0.37E+05 copy numbers per µg RNA in Ngb_{fl}-NSCs). As qRT-PCR analysis confirmed the absence of the *Ngb* transcript in Ngb_{KO}-NSCs ($P < 0.0001$) and analysis on the genome level confirmed the absence of the *Ngb-floxed* construct in Ngb_{KO}-NSCs, this NSC line was considered a valid Ngb knockout. The adherent NSC cultures obtained in this study displayed a uniform morphology and phenotypical properties such as the transcriptional expression of *Sox2, Fabp7*, *Slc1a3*, *Olig2* and *Vim*, which are well-established markers for radial glia-like neural stem cells [15]. This is in line with many literature reports suggesting that NSCs are closely related to radial glial lineages, thus describing a close relationship and common characteristics between astrocytes and NSCs [25, 28, 37]. The ability of Ngb_{fl}- and Ngb_{KO} NSCs to differentiate *in vitro* into astrocytes and neurons further support their neural stem cell identity.

To investigate if the reported neuroprotective character of Ngb would express itself in the NSC cultures, the effect of glucose deprivation on NSCs was monitored in the presence and absence of Ngb under normoxic and anoxic conditions. As previous *in vitro* studies using the human neuroblastoma cell line SH-SY5Y had shown upregulation of Ngb under OGD and even prolonged cell survival after Ngb overexpression under these conditions, we hypothesized Ngb_{KO}-NSCs to undergo increased mortality during OGD [38]. Although the shift from GD to OGD led to higher mortality rates in both cell lineages, no significant quantitative difference in cell death was monitored between Ngb_{fl}-NSCs and Ngb_{KO}-NSCs. As Ngb_{KO}-NSCs did not display an increased mortality rate as compared to Ngb_{fl}-NSCs, our results do not support the hypothesis that Ngb, under steady state expression levels in NSC, may promote protection against OGD-induced cell death. However, this conclusion may be cell-type dependent and primarily relevant for cells with low Ngb expression levels. Furthermore, Ngb's mode of action might be different in overexpression setups compared to wild type and our Ngb knockout cellular systems.

The main focus of the present study was to address a potential role of Ngb in neurodevelopment. To this end, growth patterns and proliferation of the different NSC lines were studied. Growth curve analyses clearly revealed the enhanced

growth potential of Ngb_{KO}-NSCs as compared to Ngb_{fl}-NSCs. Additionally, anti-Ki67 immunostaining, a cell marker present in active cells in late G1, S, G2 and M phase of the cell cycle, confirmed this higher proliferation capacity of Ngb_{KO}-NSCs by an increase in the occurrence of $Ki67^{+}$ nuclei of 33 % in Ngb_{KO}-NSCs compared to Ngb_{fl}-NSCs. However, no alterations in cell cycle phase distribution could be demonstrated. To identify the molecular basis of this enhanced cell growth, transcriptome analyses were performed, anticipating that differential mRNA regulation should reflect the molecular phenotype in Ngb_{KO}-NSCs versus Ngb_{fl}-NSCs. Both, a broad RNA-Seq analysis and a targeted RT^2 profiler cell cycle array revealed downregulation of the cyclin-dependent kinase inhibitor *Cdkn1a* and a pronounced upregulation of cyclin-dependent kinase *Cdk6* in Ngb_{KO}-NSCs, and both results were confirmed on the protein level. Cdkn1a is a negative regulator of cell cycle progression from G1 to S phase and acts by inhibition of Cdks (e.g. Cdk6). Cdk6 in turn facilitates the G1/S transition. In consequence, an upregulation of Cdk6 plus a downregulation of Cdkn1a may concertedly promote the progression of the cell cycle in NSCs lacking Ngb, meaning that Ngb expression in wild type cells should control cell cycle progression by a yet unknown mechanism. We note however that both, *Cdk6* and *Cdkn1a,* are targets of Tp53-mediated gene regulation [39, 40]. Tp53 signaling was indeed identified as enriched in our RNA-Seq pathway analysis. In addition, the pathway analysis also implicated the involvement of Akt signaling, based on the significant upregulation in Ngb_{KO}-NSCs of serine/threonine-protein kinase *Akt3*. Both pathways may in fact crosstalk, since Akt signaling works upstream of Tp53 [41]. Although we could not yet directly prove an influence of Ngb expression on the overall Akt, $P\text{-}Akt_{SER}$ or $P\text{-}Akt_{THR}$ levels in our NSC system, we note that Akt has recently been identified as a possible interaction partner of Ngb in neuroblastoma cells [14]. Moreover, recent studies in cancer cell models reported a regulation of the Akt pathway by Ngb [42, 43]. Guided by these interesting hypotheses, it will require extensive additional mechanistic studies to investigate the potentially subtle molecular role of Ngb in these signaling processes.

In conclusion, the current study addressed the biological role of Ngb in weakly expressing cells such as NSC. Loss of Ngb expression resulted in downregulation of Cdkn1a and upregulation of Cdk6 which lead to an enhanced cell cycle progression and increased proliferation potential of Ngb_{KO}-NSCs cells. Clearly, however, further functional investigation of the underlying molecular mechanisms are needed, as we postulate that Ngb's mode of action may involve various signaling pathways.

Acknowledgments

Prof. F. Lardon and Dr. C. Deben of the Center for Oncological Research (CORE) are thanked for helpful suggestions and the use of the humidified Bactron IV anaerobic chamber. Dr. E. Geuens is thanked for the use of the SynGene imager. E. L. and A. Q. are PhD fellows of the Fund for Scientific Research (FWO). W.V.L was a PhD fellow of the Agency for Innovation by Science and Technology (IWT, Belgium). The Fund for Scientific Research (FWO) supported this work in general (G.0687.13). T. H. acknowledges funding by the Deutsche Forschungsgemeinschaft (Ha2103/3-4) and the Johannes Gutenberg University Center for Computational Sciences (CSM/SRFN).

Author Disclosure Statement

No competing financial interests exist.

Reference List

1. Burmester T, Weich B, Reinhardt S, Hankeln T. (2000). A vertebrate globin expressed in the brain. Nature 407:520-523.

2. Burmester T, Hankeln T. (2009). What is the function of neuroglobin? J Exp Biol 212:1423-1428.

3. Dewilde S, Kiger L, Burmester T, Hankeln T, Baudin-Creuza V, Aerts T, Marden MC, Caubergs R, Moens L. (2001). Biochemical characterization and ligand binding properties of neuroglobin, a novel member of the globin family. J Biol Chem 276:38949-38955.

4. Fordel E, Thijs L, Martinet W, Lenjou M, Laufs T, Van Bockstaele D, Moens L, Dewilde S. (2006). Neuroglobin and cytoglobin overexpression protects human SH-SY5Y neuroblastoma cells against oxidative stress-induced cell death. Neurosci Lett 410:146-151.

5. Khan AA, Mao XO, Banwait S, Jin K, Greenberg DA. (2007). Neuroglobin attenuates β-amyloid neurotoxicity in vitro and transgenic alzheimer phenotype in vivo. Proc Natl Acad Sci USA 104:19114-19119.

6. Shang A, Feng X, Wang H, Wang J, Hang X, Yang Y, Wang Z, Zhou D. (2012). Neuroglobin upregulation offers neuroprotection in traumatic brain injury. Neurol Res 34:588-594.

7. Sun Y, Jin K, Mao XO, Zhu Y, Greenberg DA. (2001). Neuroglobin is up-regulated by and protects neurons from hypoxic-ischemic injury. Proc Natl Acad Sci USA 98:15306-15311.

8. Sun Y, Jin K, Peel A, Mao XO, Xie L, Greenberg DA. (2003). Neuroglobin protects the brain from experimental stroke in vivo. Proc Natl Acad Sci USA 100:3497-3500.

9. Fabrizius A, Andre D, Laufs T, Bicker A, Reuss S, Porto E, Burmester T, Hankeln T. (2016). Critical re-evaluation of neuroglobin expression reveals conserved patterns among mammals. Neuroscience 337:339-354.

10. Hümmler N, Schneider C, Giessl A, Bauer R, Walkinshaw G, Gassmann M, Rascher W, Trollmann R. (2012). Acute hypoxia modifies regulation of neuroglobin in the neonatal mouse brain. Exp Neurol 236:112-121.

11. Cutrupi S, Ferrero G, Reineri S, Cordero F, De Bortoli M. (2014). Genomic lens on neuroglobin transcription. IUBMB Life 66:46-51.

12. Chew L-J, Gallo V. (2009). The yin and yang of sox proteins: Activation and repression in development and disease. J Neurosci Res 87:3277-3287.

13. Haines B, Mao X, Xie L, Spusta S, Zeng X, Jin K, Greenberg DA. (2013). Neuroglobin expression in neurogenesis. Neurosci Lett 549:3-6.

14. Li L, Liu QR, Xiong XX, Liu JM, Lai XJ, Cheng C, Pan F, Chen Y, Yu SB, Yu ACH, Chen XQ. (2014). Neuroglobin promotes neurite outgrowth via differential binding to Pten and Akt. Mol Neurobiol 49:149-162.

15. Conti L, Pollard SM, Gorba T, Reitano E, Toselli M, Biella G, Sun Y, Sanzone S, Ying Q-L, Cattaneo E, Smith A. (2005). Niche-independent symmetrical self-renewal of a mammalian tissue stem cell. PLoS Biol 3:1594-1606.

16. Reekmans KP, Praet J, De Vocht N, Tambuyzer BR, Bergwerf I, Daans J, Baekelandt V, Vanhoutte G, Goossens H, Jorens PG, Ysebaert DK, Chatterjee S, Pauwels P, Van Marck E, Berneman ZN, Van der Linden A, Ponsaerts P. (2011). Clinical potential of intravenous neural stem cell delivery for treatment of neuroinflammatory disease in mice? Cell Transplant 20:851-869.

17. Ponsaerts P, Brown JP, Van den Plas D, Van den Eeden L, Van Bockstaele DR, Jorens PG, Van Tendeloo VFI, Merregaert J, Singh PB, Berneman ZN. (2004). Messenger RNA electroporation is highly efficient in mouse embryonic stem cells: Successful flpe- and cre-mediated recombination. Gene Ther 11:1606-1610.

18. Van den Plas D, Ponsaerts P, Van Tendeloo V, Van Bockstaele DR, Berneman ZN, Merregaert J. (2003). Efficient removal of loxp-flanked genes by electroporation of cre-recombinase mRNA. Biochem Biophys Res Commun 305:10-15.

19. McFarlane L, Truong V, Palmer JS, Wilhelm D. (2013). Novel pcr assay for determining the genetic sex of mice. Sex Dev 7:207-211.

20. Wouters A, Pauwels B, Lambrechts HAJ, Pattyn GGO, Ides J, Baay M, Meijnders P, Dewilde S, Vermorken JB, Lardon F. (2009). Chemoradiation interactions under reduced oxygen conditions: Cellular characteristics of an in vitro model. Cancer Lett 286:180-188.

21. Anders S, Huber W. (2010). Differential expression analysis for sequence count data. Genome Biol 11:106-117.

22. Wang J, Duncan D, Shi Z, Zhang B. (2013). Web-based gene set analysis toolkit (webgestalt): Update 2013. Nucleic Acids Res 41:77-83.

23. Zhang B, Kirov S, Snoddy J. (2005). Webgestalt: An integrated system for exploring gene sets in various biological contexts. Nucleic Acids Res 33:741-748.

24. Bunting KD. (2002). Abc transporters as phenotypic markers and functional regulators of stem cells. Stem Cells 20:11-20.

25. Cahoy JD, Emery B, Kaushal A, Foo LC, Zamanian JL, Christopherson KS, Xing Y, Lubischer JL, Krieg PA, Krupenko SA, Thompson WJ, Barres BA. (2008). A transcriptome database for astrocytes, neurons, and oligodendrocytes: A new resource for understanding brain development and function. J Neurosci 28:264-278.

26. Englund C, Fink A, Lau C, Pham D, Daza RAM, Bulfone A, Kowalczyk T, Hevner RF. (2005). Pax6, tbr2, and tbr1 are expressed sequentially by radial glia, intermediate progenitor cells, and postmitotic neurons in developing neocortex. J Neurosci 25:247-251.

27. Graham V, Khudyakov J, Ellis P, Pevny L. (2003). Sox2 functions to maintain neural progenitor identity. Neuron 39:749-765.

28. Hartfuss E, Galli R, Heins N, Götz M. (2001). Characterization of cns precursor subtypes and radial glia. Dev Biol 229:15-30.

29. Llorens-Bobadilla E, Zhao S, Baser A, Saiz-Castro G, Zwadlo K, Martin-Villalba A. (2015). Single-cell transcriptomics reveals a population of dormant neural stem cells that become activated upon brain injury. Cell Stem Cell 17:329-340.

30. Markó K, Kőhidi T, Hádinger N, Jelitai M, Mező G, Madarász E. (2011). Isolation of radial glia-like neural stem cells from fetal and adult mouse forebrain via selective adhesion to a novel adhesive peptide-conjugate. PLoS One 6:1-12.

31. Zhang J, Jiao J. (2015). Molecular biomarkers for embryonic and adult neural stem cell and neurogenesis. Biomed Res Int 2015:727542-727555.

32. Pesce A, Dewilde S, Nardini M, Moens L, Ascenzi P, Hankeln T, Burmester T, Bolognesi M. (2003). Human brain neuroglobin structure reveals a distinct mode of controlling oxygen affinity. Structure 11:1087-1095.

33. Brown JP, Couillard-Després S, Cooper-Kuhn CM, Winkler J, Aigner L, Kuhn HG. (2003). Transient expression of doublecortin during adult neurogenesis. J Comp Neurol 467:1-10.

34. Couillard-Despres S, Winner B, Schaubeck S, Aigner R, Vroemen M, Weidner N, Bogdahn U, Winkler J, Kuhn H-G, Aigner L. (2005). Doublecortin expression levels in adult brain reflect neurogenesis. Eur J Neurosci 21:1-14.

35. Doetsch F, Petreanu L, Caille I, Garcia-Verdugo J-M, Alvarez-Buylla A. (2002). Egf converts transit-amplifying neurogenic precursors in the adult brain into multipotent stem cells. Neuron 36:1021-1034.

36. Suh Y, Obernier K, Hölzl-Wenig G, Mandl C, Herrmann A, Wörner K, Eckstein V, Ciccolini F. (2009). Interaction between dlx2 and egfr regulates proliferation and neurogenesis of svz precursors. Mol Cel Neurosci 42:308-314.

37. Malatesta P, Appolloni I, Calzolari F. (2008). Radial glia and neural stem cells. Cell Tissue Res 331:165-178.

38. Fordel E, Thijs L, Martinet W, Schrijvers D, Moens L, Dewilde S. (2007). Anoxia or oxygen and glucose deprivation in SH-SY5Y cells: A step closer to the unraveling of neuroglobin and cytoglobin functions. Gene 398:114-122.

39. Böhlig L, Friedrich M, Engeland K. (2011). P53 activates the pank1/mirna-107 gene leading to downregulation of cdk6 and p130 cell cycle proteins. Nucleic Acids Res 39:440-453.

40. Gartel AL, Tyner AL. (1999). Transcriptional regulation of the p21(waf1/cip1)gene. Exp Cell Res 246:280-289.

41. Franke TF. (2008). Pi3k/akt: Getting it right matters. Oncogene 27:6473-6488.

42. Li Y, Dai Y-b, Sun J-y, Xiang Y, Yang J, Dai S-y, Zhang X. (2016). Neuroglobin attenuates beta amyloid-induced apoptosis through inhibiting caspases activity by activating pi3k/akt signaling pathway. J Mol Neurosci 58:28-38.

43. Zhang B, Liu Y, Li Y, Zhe X, Zhang S, Zhang L. (2017). Neuroglobin promotes the proliferation and suppresses the apoptosis of glioma cells by activating the pi3k/akt pathway. Mol Med Rep 17:2757-2763.

Tables

Table 1: Top 15 most significant up- and downregulated genes in Ngb_{KO}-NSCs.

Top 15 up-regulated DEGs			Top 15 down-regulated DEGs		
Gene ID	***P*-value**	**Fold change**	**Gene ID**	***P*-value**	**Fold change**
Igf2bp3	3.88E-09	403.7	*Anxa3*	1.79E-13	-inf.
Zdbf2	4.66E-08	+inf.	*Ddit4l*	7.51E-12	-1269.0
Comp	2.29E-07	+inf.	*Six3os1*	3.77E-10	-153.7
Fndc3c1	2.58E-07	98.5	*Trf*	1.32E-09	-57.0
Draxin	7.32E-07	44.5	*Ifit3*	3.88E-09	-79.5
Hoxa10	4.21E-06	+inf.	*Cdkn1a*	9.52E-09	-43.4
Neat1	2.15E-05	17.7	*Kcnk1*	5.56E-08	-55.3
Hes5	6.61E-05	32.2	*Fos*	5.98E-08	-34.5
Stk32b	7.27E-05	28.8	*Fosb*	8.23E-08	-42.0
Myt1	2.32E-04	37.7	*Gap43*	1.05E-07	-110.5
Trim25	4.82E-04	29.3	*Rtp4*	1.05E-07	-51.6
Col6a2	5.92E-04	44.5	*Itih5*	1.11E-07	-611.9
Shox2	6.00E-04	+inf.	*Ifit3b*	1.35E-07	-99.9
Cdk6	6.37E-04	36.7	*Mylk*	1.35E-07	-70.0
Wbscr17	7.89E-04	16.4	*Oasl2*	2.52E-07	-31.8

Genes with upregulated expression in Ngb_{KO}-NSCs are shown on the left, downregulated genes in Ngb_{KO}-NSCs are shown on the right. Genes were ranked by adjusted P-value. Inf: infinity.

Table 2: Significantly altered canonical pathways in Ngb_{KO}-NSCs compared to Ngb_{fl}-NSCs.

Ingenuity canonical pathways	*P*-value	Genes
Tp53 signaling	1.00E-03	*Ccng1*(↓),*Trp53inp1*(↓),*Cdkn1a*(↓),*Akt3*(↑), *Tnfrsf10b*(↓)
GM-CSF signaling	1.38E-03	*Ets1*(↑),*Akt3*(↑),*Stat1*(↓),*Camk2b*(↓)
Acute phase response signaling	2.09E-03	*C4b*(↓),*Fos*(↓),*Trf*(↓),*Akt3*(↑),*Serpina3n*(↓),*A2m*(↓)
Interferon signaling	2.29E-03	*Ifit3*(↓),*Irf9*(↓),*Stat1*(↓)
Jak/Stat signaling	2.40E-03	*Fos*(↓),*Cdkn1a*(↓),*Akt3*(↑),*Stat1*(↓)
Her-2 signaling in breast cancer	2.88E-03	*Cdkn1a*(↓),*Cdk6*(↓),*Alt3*(↑),*Areg*(↑)
Hepatic fibrosis / hepatic stellate cell activation	4.47E-03	*Ednrb*(↓),*Col6a2*(↓),*Csf1*(↓),*Stat1*(↓),*A2m*(↓),*Col28a1*(↓)
Aryl hydrocarbon receptor signaling	4.79E-03	*Fos*(↓),*Aldh1a1*(↑),*Nqo1*(↓),*Cdkn1a*(↓),*Cdk6*(↓)
UVA-induced MAPK signaling	4.90E-03	*Fos*(↓),*Stat1*(↓),*Parp9*(↓),*Parp14*(↓)
Glioma signaling	6.46E-03	*Cdkn1a*(↓),*Cdk6*(↓),*Akt3*(↑),*Camk2b*(↓)
HGF signaling	9.12E-03	*Ets1*(↑),*Fos*(↓),*Cdkn1a*(↓),*Akt3*(↑)
EGF signaling	9.33E-03	*Fos*(↓),*Akt3*(↑),*Stat1*(↓)
Glutamate receptor signaling	9.77E-03	*Gria1*(↓),*Gng2*(↓),*Grik2*(↑)

IPA identified 13 canonical pathways in Ngb_{KO}-NSCs. For calling significance, the Fisher's exact test was set to a P-value threshold of 0.01. Arrows indicate the direction of regulation for each gene.

Supplemental Tables

Table S1A: Overrepresented biological processes determined by Gene Ontology enrichment analysis using WebGestalt for genes upregulated in Ngb_{KO}-NSCs.

GO-Term (biological process)	GO-ID	DEGs/term [%]	DEGs/dataset [%]	*P*-value
System development	GO:0048731	0.78	48.00	5.30E-07
Anatomical structure development	GO:0048856	0.67	48.00	1.17E-05
Multicellular organismal development	GO:0007275	0.42	30.00	1.22E-05
Nervous system development	GO:0007399	1.21	34.00	2.91E-05
Anatomical structure morphogenesis	GO:0009653	1.29	48.00	3.08E-05
Developmental process	GO:0032502	0.20	16.00	1.00E-04
Skeletal system development	GO:0001501	4.14	28.00	1.00E-04
Cell development	GO:0048468	0.80	22.00	2.00E-04
Cell adhesion	GO:0007155	1.35	22.00	2.00E-04
Biological adhesion	GO:0022610	1.46	24.00	2.00E-04
Neurogenesis	GO:0022008	1.43	28.00	2.00E-04
Anatomical structure formation involved in morphogenesis	GO:0048646	1.22	36.00	4.00E-04
Cell differentiation	GO:0030154	0.67	34.00	5.00E-04
Organ development	GO:0048513	0.48	22.00	6.00E-04
Generation of neurons	GO:0048699	2.29	42.00	7.00E-04
Cellular component organization	GO:0016043	0.60	42.00	8.00E-04
Cellular component organization or biogenesis	GO:0071840	0.50	36.00	1.30E-03
Cellular developmental process	GO:0048869	0.44	24.00	1.40E-03
Tissue development	GO:0009888	0.49	12.00	1.70E-03
Embryonic organ morphogenesis	GO:0048562	3.54	16.00	2.20E-03
Cell morphogenesis involved in differentiation	GO:0000904	1.62	16.00	2.30E-03
Embryonic morphogenesis	GO:0048598	1.59	16.00	2.60E-03
Neuron projection development	GO:0031175	0.94	10.00	4.00E-03
Osteoblast differentiation	GO:0001649	6.71	20.00	4.30E-03

Embryo development	GO:0009790	1.55	28.00	4.30E-03
Regulation of multicellular organismal process	GO:0051239	0.59	22.00	5.50E-03
Regulation of multicellular organismal development	GO:2000026	2.23	52.00	6.70E-03
Single-multicellular organism process	GO:0044707	0.44	52.00	8.50E-03
Multicellular organismal process	GO:0032501	0.44	52.00	8.80E-03

Table S1B: Overrepresented biological processes determined by Gene Ontology enrichment analysis using WebGestalt for genes downregulated in Ngb$_{KO}$-NSCs.

GO-Term (biological process)	GO-ID	DEGs/term [%]	DEGs/dataset [%]	*P*-value
Innate immune response	GO:0045087	5.69	14.66	2.46E-11
Response to stress	GO:0006950	1.66	30.17	7.29E-09
Immune response	GO:0006955	2.94	17.24	2.41E-08
Cellular response to interferon-beta	GO:0035458	30.00	5.17	1.55E-07
Immune system process	GO:0002376	1.92	22.41	2.53E-07
Response to interferon-beta	GO:0035456	26.09	5.17	4.00E-07
Defense response	GO:0006952	2.46	17.24	5.35E-07
Multi-organism process	GO:0051704	2.32	15.52	1.02E-05
Response to cytokine stimulus	GO:0034097	3.49	10.34	3.67E-05
Response to other organism	GO:0051707	2.71	12.07	6.43E-05
Response to biotic stimulus	GO:0009607	2.55	12.07	1.00E-04
Cellular process	GO:0009987	0.66	75.86	2.00E-04
Response to stimulus	GO:0050896	0.83	50.00	2.00E-04
Response to interferon-alpha	GO:0035455	28.57	3.45	2.00E-04
Regulation of localization	GO:0032879	1.53	18.97	3.00E-04
Immune effector process	GO:0002252	2.88	10.34	3.00E-04
Positive regulation of biological process	GO:0048518	1.03	29.31	2.10E-03
Regulation of immune system process	GO:0002682	2.01	12.07	2.20E-03
Cellular response to cytokine stimulus	GO:0071345	3.35	7.76	2.30E-03

Regulation of cellular component movement	GO:0051270	2.38	9.48	5.20E-03
Regulation of biological process	GO:0050789	0.72	55.17	8.30E-03

GO-enrichment identified A) 29 overrepresented biological processes for up-regulated DEGs and B) 21 for down-regulated DEGs. For calling significance, the threshold for Bonferroni-adjusted P-values was set to 0.01. Each term comprises at least 4 DEGs.

Figure legends

Figure 1 Schematic presentation, validation and characterization of the Ngb knockout model. A) Schematic presentation of the gene targeting strategy starting with the endogenous *Ngb* locus (upper construct), the *Ngb-floxed* locus representing the locus of Ngb_{fl}-NSCs (middle construct) and the *Cre*-mediated excised locus representing the locus of Ngb_{KO}-NSCs (bottom construct). The solid line represents the chromosome sequence, grey-hatched rectangles represent coding exons and triangles represent *loxP* sites. Neo represents the neomycin positive selection cassette flanked by *FRT* sites. Diagram is not depicted to scale. B) Validation on gDNA level: agarose gel electrophoresis after PCR to the *Ngb* locus of Ngb_{fl}-NSCs (lane 1) and Ngb_{KO}-NSCs (lane 2). L: 1 kb ladder. C) Validation on transcript level by qRT-PCR expressed as *Ngb* copy number per µg RNA of Ngb_{fl}-NSCs and Ngb_{KO}-NSCs. Data were depicted as mean (n = 6) ± SD (**** $P < 0.0001$). D) *In vitro* differentiation potential of Ngb_{fl}-NSCs (left) and Ngb_{KO}-NSCs (right). The upper row represents staining of undifferentiated NSCs and the lower row represents staining of differentiated NSCs both with immunostaining for DAPI and GFAP in column 1 and 3 and immunostaining for DAPI, GFAP and TuJ1 in column 2 and 4. Representative images were taken from 2 independent experiments consisting both of 3 replicate stainings. Scale bar: 100 µm.

Figure 2 Principle component (A) and hierarchical cluster (B) analysis. The principle component analysis (PCA) and hierarchical cluster analysis (HCA) are based on our own NSC transcriptomes and publicly available RNA-Seq datasets from different cells types of the mouse brain: astrocytes (ACY), neurons (NEU), neural stem cells (NSC), neurospheres (NSPH), oligodendrocytes (ODC) and oligodendrocyte progenitor cells (OPC). A proper grouping of the NSCs from our study ($Ngb_{fl/KO}$-NSCs) with NSCs and NSPHs from three other, independent public RNA-Seq studies is observed.

Figure 3 Glucose deprivation of Ngb_{fl}-NSCs and Ngb_{KO}-NSCs under normoxia or hypoxia. Relative growth of Ngb_{fl}-NSCs and Ngb_{KO}-NSCs after 0, 24 and 48 hours of glucose deprivation under normoxic (GD) or anoxic (OGD) conditions. The growth at start was used to normalize (100 %). Data were depicted as mean (n = 3) ± SD. The progress in time is significantly different depending on oxygen treatment ($P < 2E\text{-}16$) but within an oxygen treatment there is no difference between the genotypes ($P = 0.42$).

Figure 4 Growth and cell cycle distribution analysis of Ngb_{fl}-NSCs and Ngb_{KO}-NSCs. A) Growth curve analysis of Ngb_{fl}-NSCs (full line) compared to Ngb_{KO}-NSCs (striped line) over 4 days. Lines connect the mean (n = 3) ± SD. The cell number at start was used to normalize (100 %). ** P < 0.01, *** P < 0.001, **** P < 0.0001. B) Percentage $Ki67^+$ stained nuclei in Ngb_{fl}-NSCs compared to Ngb_{KO}-NSCs. Data are depicted as mean (n = 14) ± SD (* P < 0.05). C) Cell cycle distribution of Ngb_{fl}-NSCs (full bars) compared to Ngb_{KO}-NSCs (white bars). DNA content was measured by flow cytometry according to the Vindelov method. Cells were divided into 3 groups according to the cell cycle phase: G0/G1 (≤2n); S (2n-4n); G2/M (4n). The percentage of cells in each phase is presented as mean (n = 3) ± SD (ns = not significant).

Figure 5 Expression levels of cell cycle genes in Ngb_{fl}-NSCs and Ngb_{KO}-NSCs. A) Relative expression levels of cell cycle genes expressed as logarithmic fold changes in Ngb_{KO}-NSCs compared to Ngb_{fl}-NSCs obtained by RNA-Seq and RT^2 array. * P < 0.05. B) Western blot to Cdk6 and Cdkn1a in Ngb_{fl}-NSC (lane 1) and Ngb_{KO}-NSC (lane 2) protein extracts. β-Actin was used as a positive control. Representative images were taken from 6 or 7 independent experiments. C) Quantification of the Western blot signal of Ngb_{fl}-NSC and Ngb_{KO}-NSC protein extracts to Cdk6 and Cdkn1a. Relative density was first normalized to β-Actin and then to the signal of the Ngb_{fl}-NSC extract. Data are depicted as mean (n = 6 for Cdk6 and n = 7 for Cdkn1a) ± SD (* P < 0.05).

Figure S1 Protein expression of Akt, P-Akt_{SER} and P-Akt_{THR} in Ngb_{fl}-NSC and Ngb_{KO}-NSC protein extracts. Western blot analysis to Akt, P-Akt_{SER} and P-Akt_{THR} in Ngb_{fl}-NSC and Ngb_{KO}-NSC protein extracts. β-Actin is used as a positive control. Lane 1: PageRuler™ Plus Prestained Protein Ladder (ThermoFisher Scientific) in kDa, Lane 2: Ngb_{fl}-NSC protein extract, Lane 3: Ngb_{KO}-NSC protein extract.

Figure 1

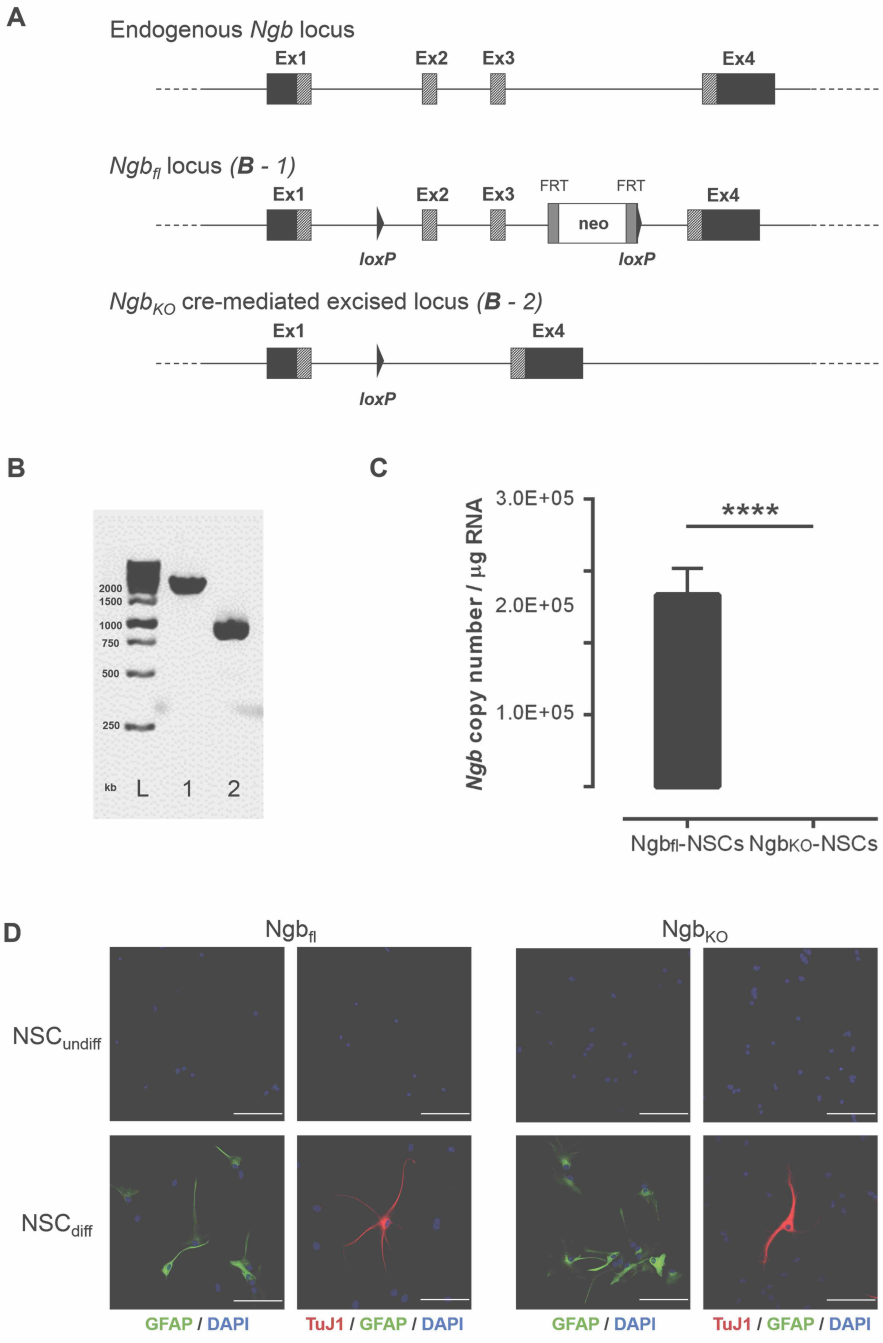
A
Endogenous Ngb locus
Ex1
Ex2
Ex3
Ex4
Ngb_fl locus (B - 1)
FRT
FRT
neo
loxP
loxP
Ngb_KO cre-mediated excised locus (B - 2)
B
2000
1500
1000
750
500
250
kb
L
1
2
C
Ngb copy number / µg RNA
3.0E+05
2.0E+05
1.0E+05
****
Ngbfl-NSCs
NgbKO-NSCs
D
Ngb_fl
Ngb_KO
NSC_undiff
NSC_diff
GFAP / DAPI
TuJ1 / GFAP / DAPI
GFAP / DAPI
TuJ1 / GFAP / DAPI

Figure 2

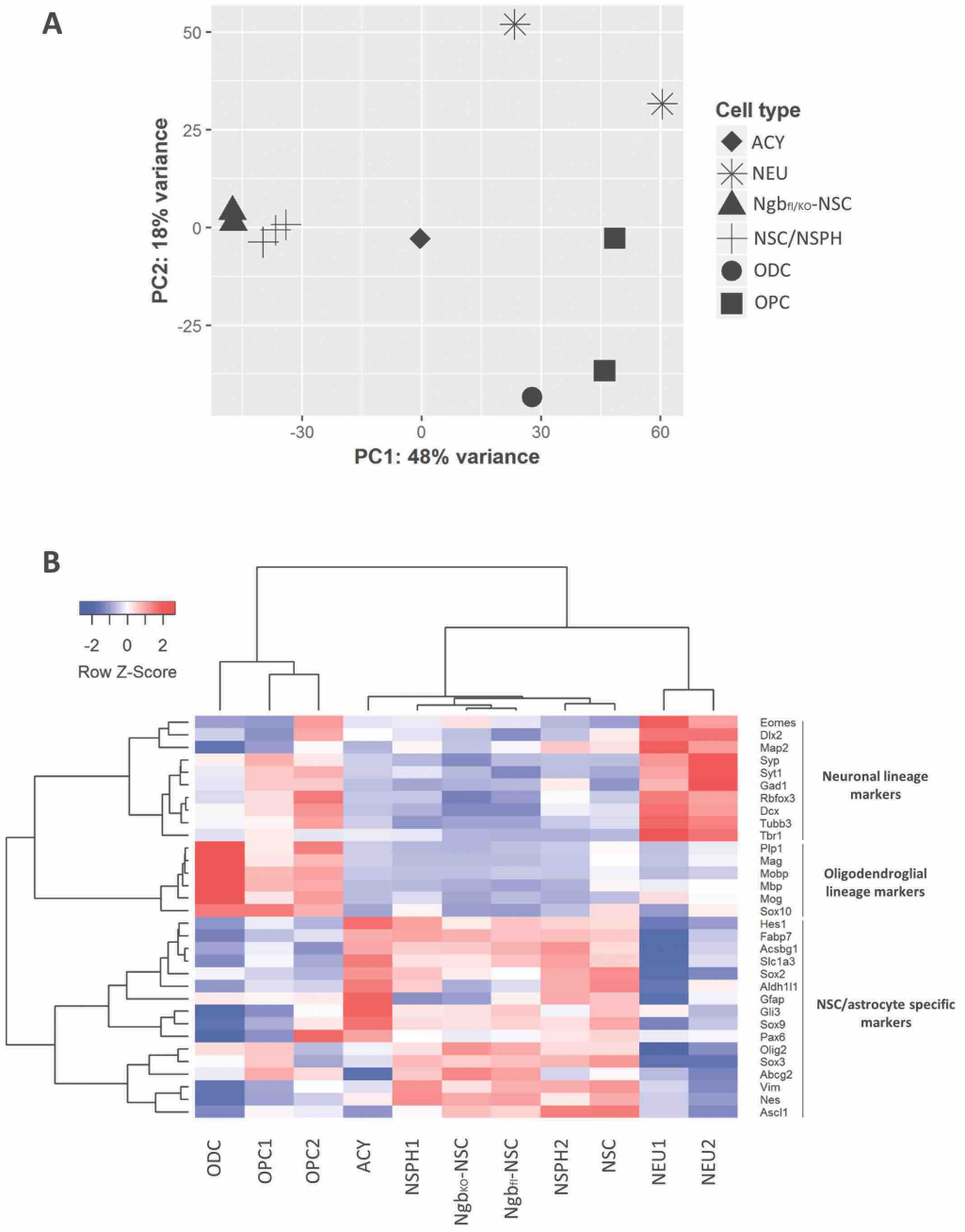
A
50
25
0
-25
PC2: 18% variance
-30
0
30
60
PC1: 48% variance
Cell type
ACY
NEU
Ngbfl/KO-NSC
NSC/NSPH
ODC
OPC
B
-2
0
2
Row Z-Score
Eomes
Dlx2
Map2
Syp
Syt1
Gad1
Rbfox3
Dcx
Tubb3
Tbr1
Plp1
Mag
Mobp
Mbp
Mog
Sox10
Hes1
Fabp7
Acsbg1
Slc1a3
Sox2
Aldh1l1
Gfap
Gli3
Sox9
Pax6
Olig2
Sox3
Abcg2
Vim
Nes
Ascl1
Neuronal lineage markers
Oligodendroglial lineage markers
NSC/astrocyte specific markers
ODC
OPC1
OPC2
ACY
NSPH1
NgbKO-NSC
NgbFl-NSC
NSPH2
NSC
NEU1
NEU2

Figure 3

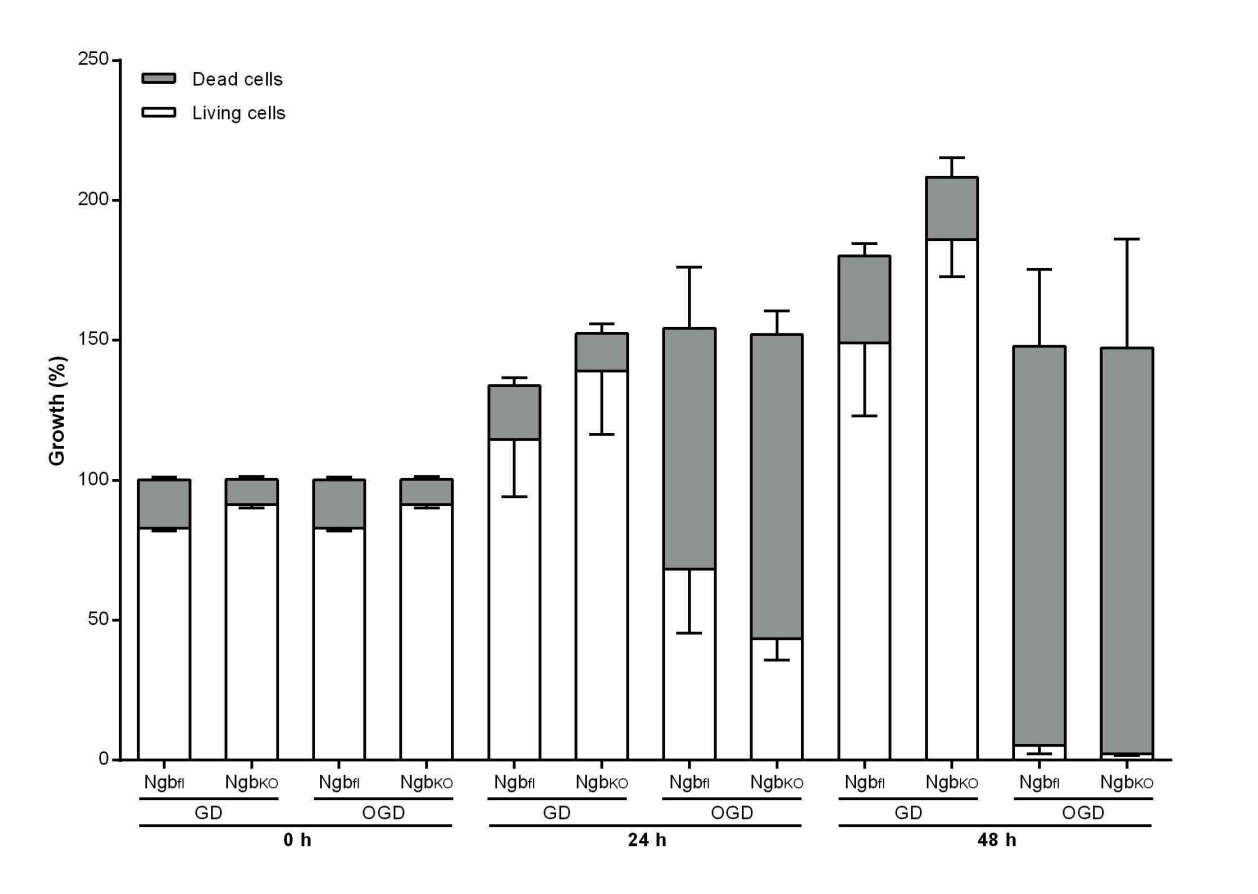
Dead cells
Living cells
Growth (%)
250
200
150
100
50
0
Ngbfl
NgbKO
GD
OGD
0 h
24 h
48 h

Figure 4

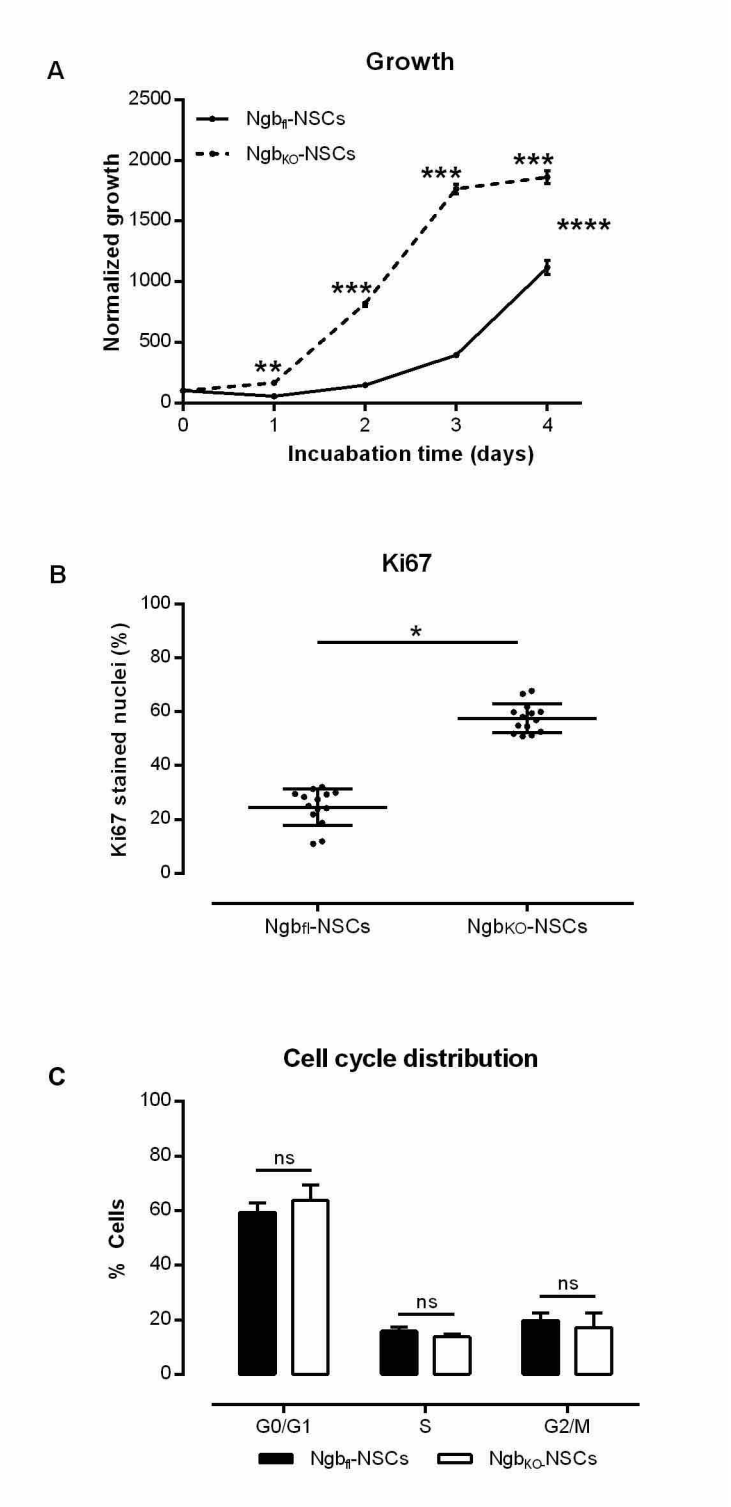
A
Growth
Ngb$_{fl}$-NSCs
Ngb$_{KO}$-NSCs
Normalized growth
Incuabation time (days)
**
***
***
***
****
B
Ki67
Ki67 stained nuclei (%)
*
Ngb$_{fl}$-NSCs
Ngb$_{KO}$-NSCs
C
Cell cycle distribution
% Cells
ns
ns
ns
G0/G1
S
G2/M
Ngb$_{fl}$-NSCs
Ngb$_{KO}$-NSCs

Figure 5

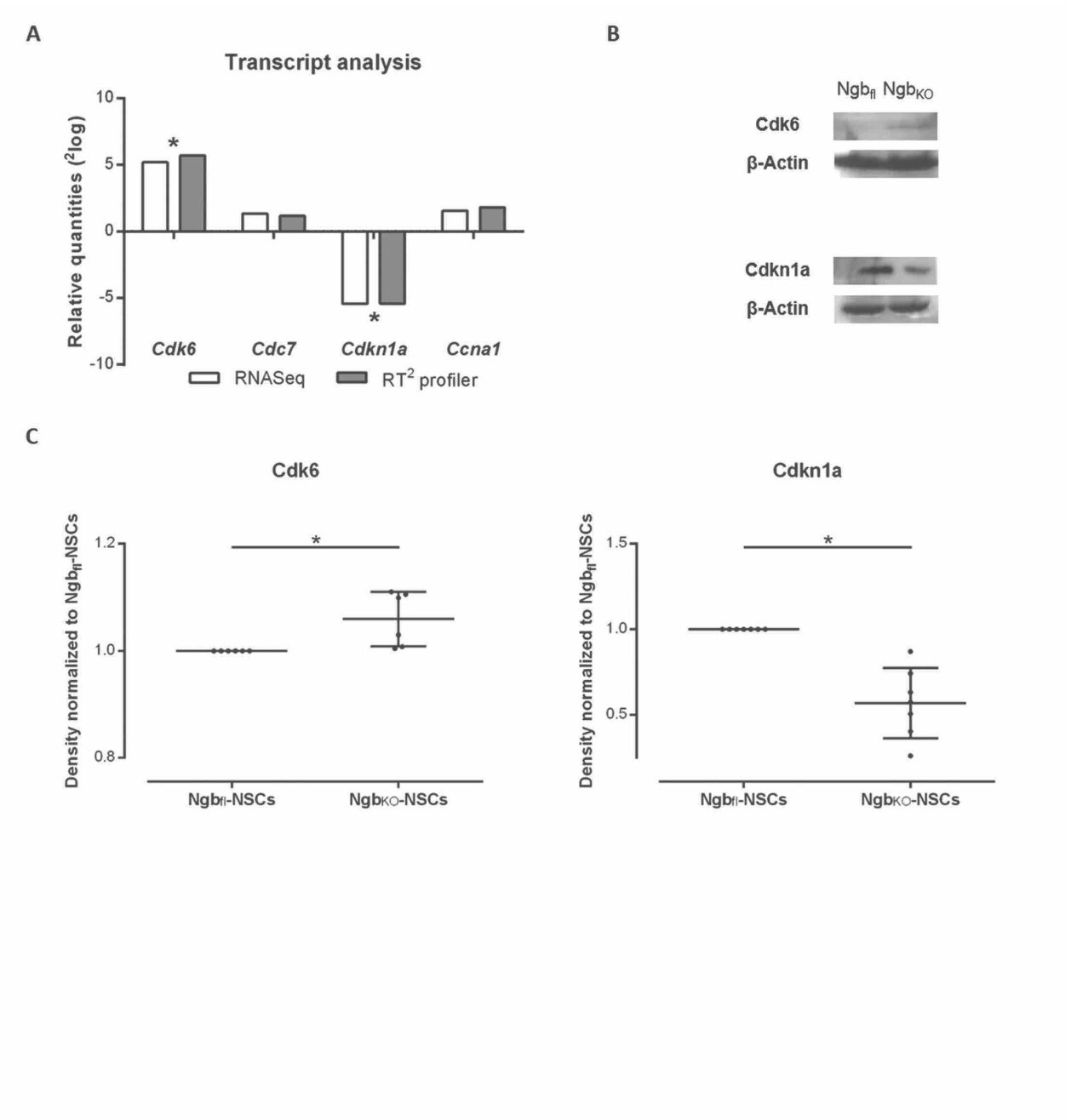
A
Transcript analysis
Relative quantities (2log)
10
5
0
-5
-10
*
*
Cdk6
Cdc7
Cdkn1a
Ccna1
RNASeq
RT2 profiler
B
Ngbfl Ngbko
Cdk6
β-Actin
Cdkn1a
β-Actin
C
Cdk6
Density normalized to Ngbfl-NSCs
1.2
1.0
0.8
*
Ngbfl-NSCs
Ngbko-NSCs
Cdkn1a
Density normalized to Ngbfl-NSCs
1.5
1.0
0.5
*
Ngbfl-NSCs
Ngbko-NSCs

Supplementary Figure S1